

Laser induced adjustment of the conductivity of rare earth doped Mn-Zn nanoferrite

S.I. EL-DEK^{1,*}, M.A. AHMED², ALAAELDIN A. ELTAWIL³, M.S. AFIFY²

¹Materials Science and Nanotechnology Department, Faculty of Post graduate studies for Advanced Sciences, (PSAS), Beni-Suef University, Beni-Suef, Egypt

²Materials Science lab (1), Physics Department, Faculty of Science, Cairo University, Giza, Egypt

³National Institute for Standard (NIS), Giza, Egypt

Two series of Mn-Zn nanoferrites (namely $Mn_{1-x}Zn_xFe_2O_4$ and $Mn_{1-x}Zn_xFe_{2-y}R_yO_4$) were synthesized using standard ceramic technique. X-ray diffraction and FT-IR were employed in the characterization of the nanopowder. The X-ray density for each sample increased after laser irradiation which was correlated with the decrease in the unit cell volume. The study involved the thermal and frequency variation of the dielectric constant and AC conductivity of the investigated samples before and after laser irradiation. The later altered the conductivity by decreasing its value for the rare earth doped samples except for the Sm^{3+} doped one. The results suggested the exploitation of Mn-Zn doped rare earth nanoferrites in many technological applications demanding high resistivity.

Keywords: rare earth nanoferrite; ceramic technique; ceramic characterizations; laser irradiation of magnetic ceramic

1. Introduction

Manganese-zinc (Mn-Zn) ferrites are important candidates for the applications in high-frequency range due to their high magnetic permeability, low magnetic losses and electrical resistivity [1]. These materials are extensively used in memory elements, microwave devices, magnetic recording media, radiofrequency coils, transformer cores and rod antennas and many other applications [2, 3]. The concentration of ferrous and ferric ions and their distribution between 4- and 6-fold sub-lattices, play a serious role in determining the magnetic and electrical properties [4] of such ferrites specially in nanoscale. Zn^{2+} dilution in ferrites appears to change both electric and magnetic properties, and promotes densification as well as grain growth [5, 6]. Ahmed et al. [7] reported that the dielectric behavior of Mn-Zn ferrite varied with sintering temperature. Mostly, in Mn-Zn ferrite, Mn-cations reside on both A and B sites [8], which makes it a partially inverse spinel. Rare earth ions could

help in tuning the physical properties of substituted Mn-Zn ferrite owing to their larger ionic radius. When these ions occupy the octahedral B-sites, they can substitute Fe^{3+} ions at low concentrations [9]. Rezlescu et al. [10] studied the effect of Fe replacement by R^{3+} ions ($R = Yb, Er, Sm, Tb, Gd, Dy, \text{ and } Ce$) on the properties of $Ni_{0.7}Zn_{0.3}Fe_2O_4$ ferrite. They established that rare earth ions enter the spinel matrix instead of small amounts of Fe^{3+} ions and have an impact on both magnetic and electrical properties of the nanoferrite. The influence of the rare earth ions on the electrical properties of spinel ferrite was interpreted [11] depending on their ionic radius. A small amount of R^{3+} ions integrated in the ferrite favor the development of the crystalline secondary phases connected with alterations in the electrical and magnetic parameters. Several researchers [12–16] examined the influence of laser irradiation and doping on the properties of bulk and thin films of ferrites. Rare earth doping effect [17, 18] on the Mg-Ti ferrite electrical properties was also examined and it was reported that the type and concentration of the 4f element take the most

*E-mail: samaa@psas.bsu.edu.eg

important part in controlling the conductivity as well as the dielectric parameters. Another study [19] aimed at comparing the effect of gamma, laser and neutron irradiation on the physicochemical properties of nanometric Mn ferrites. As a result, a decrease in the particle size and magnetic susceptibility after laser irradiation was observed, while the unit cell volume, Curie temperature, dielectric constant, loss and AC conductivity increased.

Maheshkumar *et al.* [20] irradiated a cobalt ferrite with Nd-YAG laser. They observed the creation of defects in the lattice after irradiation which affected cation distribution and structural, and magnetic properties. The lattice constant computed from XRD data for virgin and irradiated samples revealed increasing trend after irradiation. Ghazanfar *et al.* [1] showed that the lattice constant increases proportionally to the Mn content x in $Mn_xZn_{1-x}Fe_2O_4$. The experimental density of the ferrites was increased, whereas the X-ray density decreased with increasing Mn content. On the other hand, the porosity revealed a decreasing trend with the increase in manganese concentration.

In this piece of research work, we have examined the impact of laser irradiation on the electrical properties of rare earth doped Mn-Zn nanoferrites to optimize these properties. The research should help in using the well-known Mn-Zn ferrite components in versatile industrial applications.

2. Experimental

Samples with the chemical formula $Mn_{1-x}Zn_xFe_2O_4$ (where $0.1 \leq x \leq 0.7$) and $Mn_{1-x}Zn_xFe_{2-y}R_yO_4$ (where R = none, Dy^{3+} , Gd^{3+} , Sm^{3+} , Nd^{3+} and Ce^{3+}), were synthesized using double sintering ceramic technique [21]. Analar grade form oxides (BDH) MnO_2 , ZnO , Fe_2O_3 , Dy_2O_3 , Gd_2O_3 , Sm_2O_3 , Nd_2O_3 and Ce_2O_3 in stoichiometric ratios were mixed together and grinded for 3 hours using agate mortar then regrinded in agate ball mill for another 2 hours. The samples were compressed into pellets using a uniaxial hydraulic press, under a pressure of 1.6×10^8 Pa. Pre-sintering was carried out at 900 °C for 6 hours and cooling to room

temperature at the same rate as that of heating (4 °C/min). The samples were regrinded again into fine powder, and compressed again into pellets. The final sintering was carried out at 1300 °C for 10 hours in open air at the same rate in a Lenton Furnace UAF 16/5 (UK). X-ray diffraction was carried out using Philips Pu 1390 channel control with $CoK\alpha$ target to assure the formation of cubic spinel structure. The prepared samples were investigated using FT-IR spectrophotometer, model 300E, in the range of 200 cm^{-1} to 1000 cm^{-1} to study the vibration spectra and to assure the formation of the samples in a proper form. For the electrical properties measurements, the pellets were polished and the two surfaces were coated with silver paste, then checked for good conduction. The real part of dielectric constant ϵ' and the AC conductivity σ were measured using a self-calibrated Hioki LCR Hi tester, type 3531 (Japan) as a function of temperature from 300 K to 800 K in the frequency range of 100 kHz to 5 MHz. The bridge automatically collected the data using lab view-based software. The temperature of the samples was monitored using a K-type thermocouple connected to a digi-sense thermometer (USA) with junction in contact with the sample. The accuracy of measuring temperature measurement was better than ± 1 °C. Similar measurements were performed after laser irradiation using Nd-Yag laser of 1064 nm wavelength and an energy of 250 mJ, with twenty shots and pulse duration = 10 ns.

3. Results and discussion

3.1. X-ray diffraction analysis

Fig. 1 shows the XRD patterns of $Mn_{0.6}Zn_{0.4}R_{0.02}Fe_{1.98}O_4$, where R = none, Dy^{3+} , Gd^{3+} , Sm^{3+} , Nd^{3+} and Ce^{3+} before and after laser irradiation. From X-ray analysis, it is observed that the samples have the spinel structure with cubic symmetry as compared with ICDD Card Number.

$Mn_{1-x}Zn_xFe_2O_4$ samples crystallized in single phase spinel structure with cubic symmetry as compared and indexed with ICDD Card

No. 74-2402. The values of the lattice constants are reported in Table 1 for $\text{Mn}_{1-x}\text{Zn}_x\text{Fe}_2\text{O}_4$ ($0.1 \leq x \leq 0.7$) and they decrease with increasing zinc content x . This is a direct consequence of the smaller ionic radius of Zn^{2+} (0.60 Å) as compared with that of Mn^{2+} (0.66 Å), discussed in the literature [2, 22]. The X-ray density D_x was calculated using the relation [23]:

$$D_x = \frac{ZM}{Na^3} \quad (1)$$

where ($Z = 8$) is the number of molecules per unit cell, M is the molecular weight, N is Avogadro number and a is the lattice parameter. From the data in Table 1, it is observed that the X-ray density increases with the increase in Zn-content x , due to the difference in atomic weight between Mn (54.938) and that of Zn (65.37).

After laser irradiation, the diffractogram indicates stability of spinel cubic structure with appreciable shift of the planes. This is ascribed to laser interaction with the metal ions at A and B sites. Another observation in the figure is found for the plane (4 4 0) which is broad before, and changes into sharper after laser irradiation. This was expected because the heat generated from the bombardment of laser increases the crystallite size as reported in Table 2. Laser irradiation enhances the formation of Fe^{3+} according to the pattern: $\text{Laser} + \text{Fe}^{2+} \rightarrow \text{Fe}^{3+} + e^-$. The latter has a small ionic radius on both tetrahedral and octahedral coordinations and leads to a decrease in lattice parameter as can be seen in Table 2. The difference between the values of the lattice parameter in case of Dy^{3+} and Gd^{3+} is more pronounced than that for the other elements. This may be due to the difference in the diffusion mechanism and solubility limit of the R^{3+} ion in the spinel matrix. In more simpler explanation, the pinning diffusion mechanism is expected to increase the crystal size by increasing the microstrain in the outward direction. Consequently, this increases relatively the amount of pressure exerted by the secondary phase on the spinel matrix.

By comparing the intensity coming from the planes before and after laser irradiation it is observed that the planes identifying the secondary

phase (Fe_2O_3) increased after laser irradiation for all samples except for Sm^{3+} . This may be due to the decomposition that takes place as a result of heat generation by laser on the material surface (Fig. 1).

In case of Sm^{3+} ion substitution, the amount of secondary phase decreases after laser irradiation. This may be due to the partial incorporation of Sm^{3+} into the cubic spinel matrix. Additionally, the amount of heat generated from the laser photons helps Sm^{3+} ions to incorporate into the structure by pinning diffusion which results in a decrease in the secondary phase intensity. The data in Table 2 show that, after laser irradiation the density of the samples increases with increasing the ionic radius of the rare earth element with similar trend as that before laser irradiation. Looking closer to the data, it is noticed that the X-ray density for each sample increases after laser irradiation which can be correlated to the decrease in the unit cell volume.

3.2. IR spectral analysis

The data reported in Table 1 give the four fundamental active bands appearing in FT-IR, designated as ν_1 , ν_2 , ν_3 and ν_4 . The first two bands: ν_1 , ν_2 , appearing at about 550 cm^{-1} and 420 cm^{-1} , respectively, belong to the high frequency bands. These bands [18, 19] can be assigned to the stretching vibrations of the metal ions (Fe^{3+}) on both tetrahedral and octahedral sites. The change in the position of these bands is mainly due to the change in the $\text{Fe}^{3+}-\text{O}^{2-}$ distances on both A and B sites due to the increase in Zn content. This is confirmed by the decrease in the lattice parameter with increasing Zn content. The appearance of a shoulder at about 340 cm^{-1} is the evidence of the existence of divalent metal ions on the octahedral sites. The band ν_4 at about 220 cm^{-1} is accompanied by a shoulder at $\sim 260 \text{ cm}^{-1}$ which is assigned to the lattice vibrations. The broadening of ν_2 band is mainly due to the existence of more than one type of metal ions on the octahedral sites [19].

The transmission bands of FT-IR spectra of $\text{Mn}_{0.6}\text{Zn}_{0.4}\text{R}_{0.02}\text{Fe}_{1.98}\text{O}_4$ before and after laser irradiation are reported in Table 2. From the table, it is noted that the IR spectrum

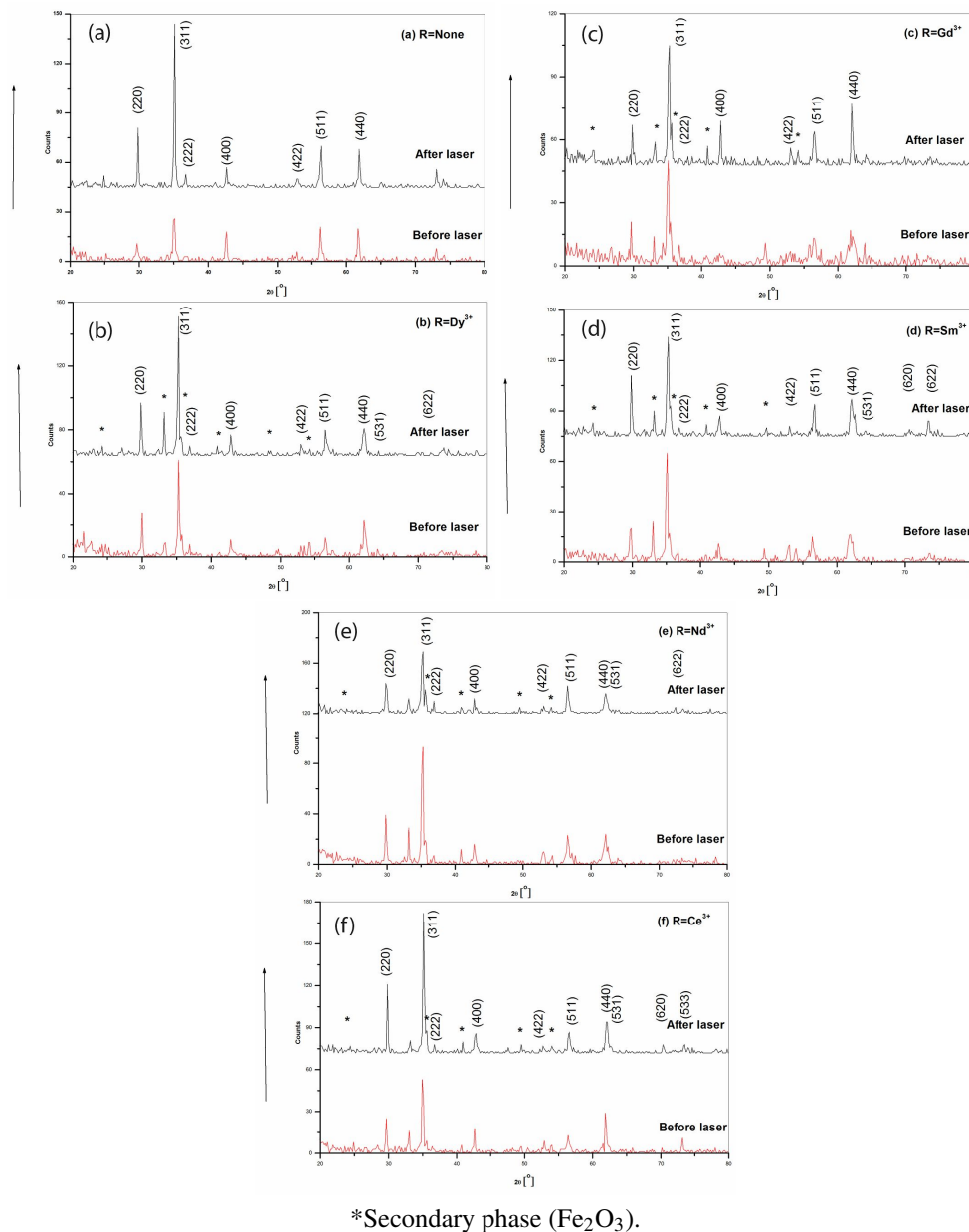


Fig. 1. XRD patterns of $\text{Mn}_{0.6}\text{Zn}_{0.4}\text{R}_{0.02}\text{Fe}_{1.98}\text{O}_4$: (a) $\text{Mn}_{0.6}\text{Zn}_{0.4}\text{Fe}_2\text{O}_4$; (b) $\text{Mn}_{0.6}\text{Zn}_{0.4}\text{Dy}_{0.02}\text{Fe}_{1.98}\text{O}_4$; (c) $\text{Mn}_{0.6}\text{Zn}_{0.4}\text{Gd}_{0.02}\text{Fe}_{1.98}\text{O}_4$; (d) $\text{Mn}_{0.6}\text{Zn}_{0.4}\text{Sm}_{0.02}\text{Fe}_{1.98}\text{O}_4$; (e) $\text{Mn}_{0.6}\text{Zn}_{0.4}\text{Nd}_{0.02}\text{Fe}_{1.98}\text{O}_4$; (f) $\text{Mn}_{0.6}\text{Zn}_{0.4}\text{Ce}_{0.02}\text{Fe}_{1.98}\text{O}_4$.

of $\text{Mn}_{0.6}\text{Zn}_{0.4}\text{R}_{0.02}\text{Fe}_{1.98}\text{O}_4$ exhibits four bands in the range of 200 cm^{-1} to 1000 cm^{-1} . Such bands are generally observed for ordered spinel ferrites [24]. The remarkable change is caused by rare earth substitution, i.e. by comparing the R^{3+} doped samples with the undoped one.

By introducing R^{3+} ions into the spinel matrix, one could expect that more than one way

of diffusion could occur. For the R^{3+} ions with small radii, a volume diffusion mechanism is the most probable. This results from the increase in the lattice parameter by introducing Dy^{3+} ions. Increasing the ionic radius of the R^{3+} may result in a pinning diffusion on the grain boundaries leading to a relatively slight compression of the spinel lattice. For larger rare earth ions, surface diffusion is

Table 1. Lattice parameter, theoretical density and IR bands positions of $(\text{Mn}_{1-x}\text{Zn}_x\text{Fe}_2\text{O}_4)$; where $0.1 \leq x \leq 0.7$.

Zn content x	a [Å]	D_x [g·cm ⁻³]	ν_1 [cm ⁻¹]	ν_2 [cm ⁻¹]	ν_{3-s} [cm ⁻¹]	ν_4 [cm ⁻¹]
0.1	8.500	5.010	554	418	333	250 S, 222
0.2	8.491	5.047	553	402	334	268 S, 222
0.3	8.479	5.092	553	418	343	259 S, 223
0.4	8.491	5.094	553	402 broad	331	262, 223
0.5	8.473	5.148	551	403	334	263, 222
0.6	8.462	5.192	553	420	340	250 S, 222
0.7	8.456	5.226	552	417	334	259 S, 222

S: shoulder.

Table 2. Lattice parameter, theoretical density and IR band positions of $\text{Mn}_{0.6}\text{Zn}_{0.4}\text{R}_{0.02}\text{Fe}_{1.98}\text{O}_4$ before and after laser irradiation; where R = None, Dy³⁺, Gd³⁺, Sm³⁺, Nd³⁺ and Ce³⁺.

R	A [Å]	L [nm]	D_x [g·cm ⁻³]	ν_1 [cm ⁻¹]	ν_2 [cm ⁻¹]	ν_3 [cm ⁻¹]	ν_{3-s} [cm ⁻¹]	ν_{4-s} [cm ⁻¹]	ν_4 [cm ⁻¹]	
None	before	8.487	113.0	5.100	550	400	–	331	263	–
	after	8.476	159.4	5.119	549	–	392	328	–	223
Dy ³⁺	before	8.497	57.2	5.129	568	451	–	343	262	–
	after	8.470	84.1	5.178	568	453	–	337	–	–
Gd ³⁺	before	8.489	34.3	5.140	570	454	–	340	262	–
	after	8.448	75.9	5.217	569	456	–	337	259	220
Sm ³⁺	before	8.468	60.5	5.177	581	454	–	362	259	–
	after	8.470	73.3	5.172	570	454	–	346	264	221
Nd ³⁺	before	8.474	58.3	5.163	567	452	–	340	259	–
	after	8.470	60.9	5.168	568	453	–	343	–	221
Ce ³⁺	before	8.466	97.1	5.175	567	450	–	350	259	–
	after	8.458	78.5	5.190	566	448	–	346	259	220

predominant and a decrease in the lattice parameter is more pronounced. The stretching vibrations of $\text{Fe}^{2+}-\text{O}^{2-}$ and/or $\text{Mn}^{2+}-\text{O}^{2-}$ in 6-f coordination alter their positions depending on the type of R^{3+} ion due to the corresponding change in the octahedral site radius related with the ionic radius of the R^{3+} ion. It is observed that some transmission bands disappear after irradiation. This could be explained as follows: Laser irradiation shifts some ions of small size to interstitial positions in the crystal lattice. However, the appearance of the four bands for the laser irradiated sample confirms the stability of the spinel cubic structure.

3.3. Dielectric constant ϵ' and dielectric loss factor ϵ''

Fig. 2 illustrates the dependence of dielectric constant ϵ' on Zn content. One can find that ϵ''

decreases with increasing Zn content which is an acceptable result. The direct reason is that the Zn^{2+} ion decreases the Mn^{2+} ion content on the A site, thereby decreasing the polarization as well as ϵ' .

Fig. 3a shows the variation of the real part of dielectric constant ϵ' with the absolute temperature as a function of frequency for the sample $\text{Mn}_{0.6}\text{Zn}_{0.4}\text{Fe}_2\text{O}_4$. The figure illustrates that ϵ' increases with increasing temperature and decreases with increasing frequency, which is the general trend for the ferrite samples [25–28]. After laser irradiation, the values of the dielectric constant increase as shown in Fig. 3b owing to the redistribution of metal cations on equivalent crystallographic lattice sites. Moreover, an additional sharp peak appears at $T \approx 485$ K.

Table 3 reports the peak values (maximum measured values) of ϵ' and ϵ'' before and after laser

irradiation for different rare earth doped samples. The reported data indicate that a decrease in ϵ' takes place after laser irradiation which is due to the defects generated in the samples. For the values of ϵ'' , it is clear that a large value is obtained in case of Ce doped sample which is an expected result due to the existence of cerium in two valence states, namely Ce^{3+} and Ce^{4+} [29, 30]. The electron affinity and electronegativity for the different rare earth elements play a weighty and an important role in the dielectric behavior of the rare earth doped samples.

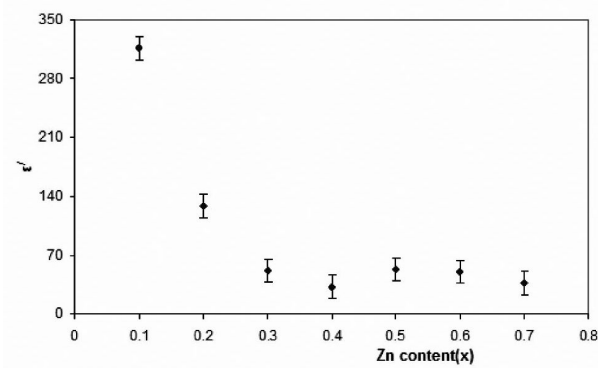


Fig. 2. Dependence of dielectric constant ϵ' on Zn content at $T = 300$ K, $f = 800$ kHz.

Fig. 4 illustrates the dependence of ϵ' on the ionic radius of R^{3+} before and after laser irradiation. One can see the high value of ϵ' maximum for the Gd^{3+} doped sample, where its ionic radius is 0.938 \AA . This was expected, because the Gd has a half filled ($4f^7$), orbital. The seven electrons are unpaired, giving larger polarization as well as larger value of ϵ' . Additionally, the large value of ϵ' for Ce may be due to its existence in different valences ($\text{Ce}^{3+} \leftrightarrow \text{Ce}^{4+}$). This activates the hopping process as well as the polarization mechanism because the dielectric constant and conductivity are of the same origin. It was expected that, the replacement of rare earth elements on the expense of Fe^{3+} on octahedral sites and laser irradiation of the samples initiate vacancies, which in turn, produce microstrain inside the sample. This means that these vacancies trap some of the electrons participating in the electrical conductivity. Thereby, the conductivity is decreased after laser irradiation.

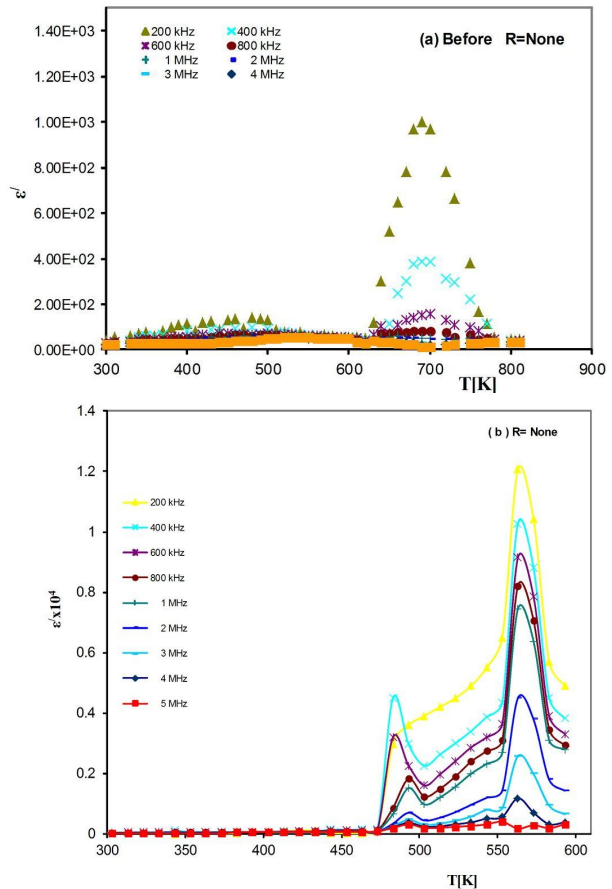


Fig. 3. Correlation between the real part of dielectric constant ϵ' of $\text{Mn}_{0.6}\text{Zn}_{0.4}\text{Fe}_2\text{O}_4$ ferrite sample and absolute temperature (a) before and (b) after laser irradiation.

Fig. 5 confirms our expectation about the decrease in the conductivity as it has the same origin as ϵ' . Laser irradiation delayed the polarization process, and ϵ' decreased as in Fig. 4. Similar behavior is observed for ϵ'' after laser irradiation as reported in Table 3.

3.4. AC conductivity

Table 4 shows the values of room temperature AC conductivity for the samples containing different Zn content at $f = 800$ kHz. The conductivity increases with Zn content below $x = 0.4$ due to the enhancement of the AA hopping between ($\text{Mn}^{3+} \leftrightarrow \text{Mn}^{2+} + e^+$) in addition to the well-know Verwey mechanism [31]. The increase in Zn content above $x = 0.4$ leads to a decrease

Table 3. Peak (maximum) values of ϵ' and ϵ'' at $f = 400$ kHz for different rare earth doped samples before and after laser irradiation.

Sample	ϵ' before	ϵ' after	ϵ'' before	ϵ'' after
None	3.86×10^2	1×10^4	–	–
Dy ³⁺	8.31×10^2	60.45	4.5×10^3	3.33×10^2
Gd ³⁺	8.01×10^2	4.73×10^2	4.69×10^3	4.13×10^3
Sm ³⁺	3.52×10^2	1.36×10^2	2.37×10^3	1.37×10^3
Nd ³⁺	1.47×10^3	6.55×10^2	7.77×10^3	5.67×10^3
Ce ³⁺	4.42×10^3	6.93×10^2	17.8×10^3	6.94×10^3

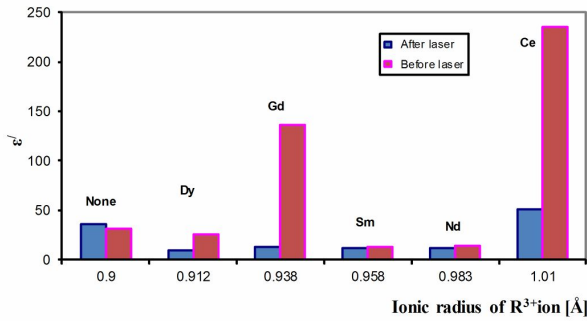


Fig. 4. Dependence of dielectric constant ϵ' on ionic radius of rare earth elements before and after laser irradiation at $T = 313$ K, $f = 800$ kHz.

in the conductivity, i.e. the resistivity increases. This is a consequence of the decrease in ($\text{Fe}^{2+}/\text{Fe}^{3+}$) ratio on B sites lowering the number of available hopping electrons, thus reducing the conductivity.

Fig. 5 illustrates the dependence of AC conductivity on the ionic radius of the rare earth element before and after laser irradiation at $f = 800$ kHz and $T = 313$ K.

The data in the figure show that after laser irradiation the conductivity decreases for the samples irrespective of their type except for Sm^{3+} substituted sample. The relative percentage change in the conductivity as a result of laser irradiation has been calculated using equation 2 and is shown in Table 5:

$$\frac{\Delta\sigma}{\sigma_{\text{before}}} = \frac{\sigma_{\text{after}} - \sigma_{\text{before}}}{\sigma_{\text{before}}} \times 100 \quad (2)$$

The absolute value of the relative percentage change for the undoped sample is 30, which is

considered as the minimum value while for the Ce doped sample it reaches 91. This decrease in the conductivity points to a large increase in the resistivity and encourages us to recommend the use of such rare earth ferrites for achieving better results including higher resistivity and lower losses, for core transformer applications and in different electronic industries at this temperature. Consequently, doping with rare earth elements with very small concentration ($x = 0.02$) instead of iron ions in $\text{Mn}_{0.6}\text{Zn}_{0.4}\text{Fe}_2\text{O}_4$ together with laser irradiation could serve for lowering the cost and enhancing the performance of existing Mn-Zn cores by increasing their resistivities.

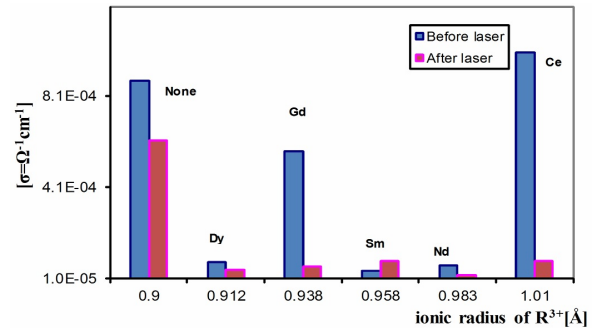


Fig. 5. Dependence of AC conductivity on the ionic radius of the rare earth elements before and after laser irradiation at $T = 313$ K, $f = 800$ kHz.

4. Conclusions

(1) $\text{Mn}_{1-x}\text{Zn}_x\text{Fe}_2\text{O}_4$ ($0.1 \leq x \leq 0.7$) and $\text{Mn}_{0.6}\text{Zn}_{0.4}\text{R}_{0.02}\text{Fe}_{1.98}\text{O}_4$; ($\text{R} = \text{none}, \text{Dy}^{3+}, \text{Gd}^{3+}, \text{Sm}^{3+}, \text{Nd}^{3+}$ and Ce^{3+}) nanoparticles were successfully prepared by standard ceramic method.

Table 4. Dependence of (σ) on Zn content at T = 300 K, f = 800 kHz.

Zn content x	$\sigma \times 10^{-4} [\Omega^{-1} \cdot \text{cm}^{-1}]$
0.1	4.0
0.2	6.9
0.3	12.2
0.4	6.5
0.5	10.1
0.6	7.5
0.7	4.3

Table 5. Values of laser induced change in the conductivity % at f = 800 kHz and T = 313 K for different rare earth doped samples.

Sample	$\frac{\Delta\sigma}{\sigma_{\text{before}}} \%$
None	-30
Dy ³⁺	-41
Gd ³⁺	-89
Sm ³⁺	94
Nd ³⁺	-65
Ce ³⁺	-91

(2) By increasing Zn content the lattice parameter and porosity decreased while the X-ray density increased.

(3) The effect of laser irradiation on the nanoferrites under investigation is as follows:

– Laser irradiation increases the crystal size of the samples and decreases the dielectric constant and dielectric loss factor.

– After laser irradiation the conductivity of the samples decreases irrespective of the type of rare earth used except for Sm³⁺.

– The decrease in the conductivity is connected with a large improvement in the resistivity and encourages us to recommend the use of ferrites after laser irradiation to achieve higher resistivity and lower losses for core transformer applications and as advanced functional material.

– Doping with small amount of rare earth elements (1 %) on the expense of iron ions in Mn_{0.6}Zn_{0.4}Fe₂O₄ together with laser irradiation

could serve to lowering the cost of existing Mn-Zn cores in addition to their low losses and improved performance.

References

- [1] GHAZANFAR U., SIDDIQI S.A., ABBAS G., *Mater. Sci. Eng. B-Adv.*, 118 (2005), 84.
- [2] ABBAS T., KHAN Y., AHMAD M., ANWAR S., *Solid. State. Commun.*, 82 (1992), 701.
- [3] SNELLING E.C., *Soft Ferrites Properties and Applications*, 2nd Ed., Butter Worth-Heinemann, London, 1988.
- [4] ATEIA E., AHMED M.A., EL-AZIZ A.K., *J. Magn. Magn. Mater.*, 31 (2007), 545.
- [5] SOLYMAN S., *Ceram. Int.*, 32 (2006), 755.
- [6] DAS P.S., SINGH G.P., *J. Magn. Magn. Mater.*, 401 (2016), 918.
- [7] AHMED M.A., EL-KHAWAS E.H., RADWAN F.A., *J. Mater. Sci.*, 36 (2001), 1.
- [8] AHMED M.A., AZAB A.A., EL-KHAWAS E.H., *Synth. React. Inorg. M.*, 46, 3 (2016), 376.
- [9] REZLESCU E., REZLESCU N., PASNICU C., CRAUS M.L., POPO P.B., *Cryst. Res. Technol.*, 31, 3 (1996), 343.
- [10] REZLESCU N., REZLESCU E., *Solid. State. Commun.*, 88, 2 (1993), 139.
- [11] AHMED M.A., OKASHA N., EL-SAYED M.M., *Ceram. Int.*, 3 (2007), 49.
- [12] AHMED M.A., KHALIL A.A.I., SOLYMAN S., *J. Mater. Sci.*, 42 (2007), 4098.
- [13] TASHTOUSH N.M., *Am. J. Appl. Phys.*, 2 (2005), 887.
- [14] ELTABEY M.M., AGAMI W.R., MOHSEN H.T., *J. Adv. Res.*, 5 (5) (2014), 601.
- [15] ZHAO L., YANG H., YU L., CUI L., ZHAO X., FENG S., *J. Magn. Magn. Mater.*, 305, 1 (2006), 91.
- [16] MASTAI Y., *Advances in Crystallization Processes*, In-Tech, 2012.
- [17] AHMED M.A., ATEIA E., EL-DEK S.I., *Mater. Lett.*, 57 (2003), 4256.
- [18] AHMED M.A., ATEIA E., EL-DEK S.I., *Vib. Spectrosc.*, 30 (2002), 69.
- [19] AHMED M.A., EL-DEK S.I., MANSOUR S.F., OKASHA N., *Solid. State. Sci.*, 13 (2011), 1180.
- [20] MAHESHKUMAR L.M., VINOD N.D., SUNDAR R., RANGANATHAN K., OAK S.M., SHENGULE D.R., *Appl. Surf. Sci.*, 257 (20) (2011), 8511.
- [21] VALENZUELA R., *Magnetic Ceramics*, Cambridge University Press, Cambridge, 1994.
- [22] GOLDMAN A., *Modern Ferrite Technology*, 2nd Ed., Springer, Pittsburgh, 2006.
- [23] AHMED M.A., OKASHA N., EL-DEK S.I., *Nanotechnology*, 19 (6) (2008), 065603.
- [24] VENKATARAJU C., PAULSINGH R., *J. Nanosci.*, 2014, (2014).
- [25] MISRA N.K., SATI R., CHOWDHARY R.N.P., *Mater. Lett.*, 24 (5) (1995), 313.
- [26] BERA S., CHOWDHARY R.N.P., *Mater. Lett.*, 22, (3 – 4) (1995), 197.

-
- [27] YADAV K.L., CHOWDHARY R.N.P., *Mater. Lett.*, 19 (5) (1994), 291.
- [28] UZMA G., *Indian J. Pure. Ap. Phy.*, 53, 4 (2015), 271.
- [29] VENKATARAJU C., PAULSINGH R., *Nano-Micro Lett.*, 5 (4) (2013), 223.
- [30] KUMAR K., REDDY A., RAVINDER D., *J. Magn. Mater.*, 263 (1 – 2) (2003), 121.
- [31] MCKINNON W.R., HURD C.M., SHIOZAKI I., *J. Phys. C*, 14 (1981), L877.

Received 2016-11-04

Accepted 2017-09-20